Video-Consistent Synthetic Skiing Trajectories

M'Saydez Campbell[1]
m.saydez.campbell@univ-st-etienne.fr

Christophe Ducottet[1]
ducottet@univ-st-etienne.fr

Damien Muselet[2]
damien.muselet@univ-lr.fr

Rémi Emonet[1,3,4]
remi.emonet@univ-st-etienne.fr

[1]Université Jean Monnet, CNRS, Institut d'Optique Graduate School,
Laboratoire Hubert Curien UMR 5516, St-Etienne F-42023, France
[2]L3i, La Rochelle University, La Rochelle, 17000, France
[3]Inria
[4]Institut Universitaire de France (IUF)

Abstract

Annotated skier trajectories are essential for developing video-based methods for tracking and behavior analysis on ski slopes, but obtaining such data is costly and labor-intensive. In this work, we proposed a framework for generating synthetic skier trajectories using an extended cellular automaton model enriched with skier-specific behavior and local multi-skier anticipation. The simulated trajectories were embedded in a 3D slope representation and projected into 2D image space through a virtual pinhole camera model, enabling video-consistent synthetic observations from multiple viewpoints. We evaluated the proposed approach through skier efficiency analysis, low-level trajectory distribution comparison with the Slope-Track dataset, and multi-object tracking experiments using DeepEIoU [7] with GlideTrack [3]. The results showed that the simulated trajectories reproduced the dominant motion characteristics of real skier trajectories and that incorporating synthetic data during training improved tracking association performance on real ski-slope sequences. These findings suggest that behavior-aware synthetic trajectory generation can provide a useful complement to manually annotated ski-slope video datasets. The code can be found here.

1. Introduction

There is an increasing need for annotated trajectory data from videos of winter sports such as skiing. Such data are essential for designing algorithms to understand motion, recognize behaviors, and assess safety in slope environments. They are especially useful for learning trajectory models for tracking algorithms. However, acquiring trajectories requires extensive manual annotation, which is both time-consuming and costly. These challenges motivate the use of synthetic trajectory generation as an efficient alternative. Effective synthetic generation relies on modeling people's underlying dynamics so that realistic trajectories emerge from simulated behavior. By encoding rules governing motion, interactions, and environmental constraints, these methods can produce trajectories that reflect plausible movement patterns. Existing approaches can be broadly categorized into artificial intelligence–based models and physics- or agent-inspired simulation models.

Artificial intelligence–based methods have been increasingly applied to simulate pedestrian and crowd dynamics. For example, Lu *et al*. [10] introduced a human–AI interactive framework for smart evacuation analysis in large-scale, high-density infrastructures. Beyond evacuation scenarios, deep learning has been leveraged to address data scarcity and improve behavioral realism. Kim and Jang [9] proposed a deep learning–based framework for synthetic trajectory generation while preserving privacy, and Jiang *et al*. [8] developed a neural network approach to simulate pedestrian turning flows, capturing complex local interactions and directional changes. Despite their expressiveness, AI-based approaches generally require large volumes of annotated training data and often struggle to generalize beyond the distributions present in the training scenes or camera viewpoints. In addition, these models tend to lack interpretability and offer limited control over environmental or motion constraints.

Other methods for modeling and simulating pedestrian movements are physics-based models, queuing network models, multi-agent models and cellular-based models. Physics-based models [16, 18, 19] represent pedestrians

as individual entities whose motion is governed by predefined physical or social forces. Queuing network models [5, 15] use priority rules and probabilistic mechanisms to reproduce pedestrian flows. Multi-agent models [15] simulate dynamics through autonomous agents with individual goals and preferences, capable of interacting and cooperating within a shared environment. Cellular-based models [1, 12] discretize space into a grid of cells representing free space, obstacles, or other environmental attributes, and govern movement via local transition rules. These methods provide interpretability and explicit control, making them particularly suitable for modeling new or unseen environments.

In this work, we improve over the cellular automaton (CA) proposed in Zhang and Xie [17]. The cellular automaton incorporates transition factors based on environmental and behavioral forces to simulate skier behavior on the ski slope. We propose a refined skier behavior modeling that includes skier level and anticipation of multi-person interactions. To make these simulations consistent with real, video-based data, we do the modeling in 3D, and project them to 2D using a virtual camera model.

The main contributions of our work are:

1. **Enhanced behavior modeling** within a cellular automaton framework, capturing multi-person interactions and variable skier dynamics.
2. **Multi-view trajectory generation** that produces synthetic trajectories consistent with different camera viewpoints through a 3D slope representation and camera projection model.
3. **Demonstration that synthetic trajectory pretraining improves video tracking association performance on real ski-slope sequences.**

The remainder of the paper is organized into four sections. Section 3 presents a brief description of the existing cellular automaton model, behavior-enriched transition rules, and the generation of continuous, video-consistent trajectories. Section 4 evaluates the proposed approach through quantitative metrics, qualitative visualizations, and ablation studies. Section 5 concludes the paper with a discussion of key findings, limitations, and future directions.

2. Problem Formulation

We address the problem of generating synthetic skier trajectories for video-based applications. Given a ski slope environment and a set of skier interaction settings, the goal is to generate trajectories that (i) reflect plausible skier behavior and (ii) can be consistently projected into image space to align with video observations from one or more camera viewpoints.

2.1. Problem Definition

Formally, a skier trajectory is defined as a time-ordered sequence of positions

$$\mathcal{T} = \{\mathbf{x}_t\}_{t=1}^{T}, \quad \mathbf{x}_t \in \mathbb{R}^3, \tag{1}$$

where $\mathbf{x}_t = (x_t, y_t, z_t)$ denotes the skier's 3D position in world coordinates at time step t. The trajectory length T corresponds to the time step at which the skier reaches the end of the slope.

For a scene containing N skiers, the full trajectory set is given by

$$\mathcal{S} = \{\mathcal{T}^i\}_{i=1}^{N}. \tag{2}$$

The objective is to generate $\mathcal{S}$ such that each trajectory obeys individual motion dynamics, interaction constraints between skiers, and environmental constraints imposed by the slope geometry. Let $\mathcal{G}$ denote the slope geometry and $\mathcal{I}_t^i$ the local interaction state of skier i at time t (e.g., capturing neighboring skiers' positions). The trajectory evolution can be expressed as

$$\mathbf{x}_{t+1}^i = f\left(\mathbf{x}_t^i, \mathcal{I}_t^i, \mathcal{G}, \boldsymbol{\theta}\right), \tag{3}$$

where $f(\cdot)$ is the transition function defined by the simulation model and $\boldsymbol{\theta}$ represents environmental and behavioral factors such as friction and inertia.

In addition, the generated trajectories must support projection into the image plane to produce video-consistent observations suitable for downstream tasks such as tracking, behavior analysis, and data augmentation.

2.2. Assumptions and Scope

We assume a known slope geometry $\mathcal{G}$ represented as a base surface combined with local terrain variability. The base plane is characterized by a global inclination angle α and a steepest descent unit direction $\mathbf{d} \in \mathbb{R}^2$, with $\|\mathbf{d}\| = 1$. Terrain is represented by a discrete height map rather than an explicit slope function.

The skier's motion is assumed to be primarily aligned with the downhill direction of the base plane, with lateral deviations governed by behavioral and interaction-driven factors. Cameras are assumed to be static and calibrated, with known intrinsic parameters $\mathbf{K}$ and extrinsic parameters $(\mathbf{R}, \mathbf{t})$. Interactions are restricted to local multi-skier scenarios, emphasizing anticipatory behavior, spacing, and smooth avoidance rather than rare extreme events such as collisions. The scope of this work is synthetic trajectory generation rather than full visual rendering.

3. Framework Description

This section presents the framework for skier trajectory generation, including the existing cellular automaton, the proposed behavior-based extensions, and methods for gener-

ating trajectories that are consistent across multiple viewpoints and videos.

3.1. Review of Baseline CA Skiing Model

The framework proposed by Zhang and Xie [17] models the skier as a single particle moving on a two-dimensional cellular grid aligned with the slope. The slope is discretized into square cells of size $0.5\,\mathrm{m} \times 0.5\,\mathrm{m}$. Let M denote the slope width (lateral direction) in grid cells and J denote the slope length (downhill direction) in grid cells.

At time t, the skier occupies cell (i, j), where $i \in [0, M]$ represents the lateral position across the slope and $j \in [0, J]$ represents the downhill position. A candidate next position is denoted by (i', j'), corresponding to a movement from (i, j) to $(i + \Delta i, j + \Delta j)$. At each time step, the skier may move to one of five adjacent cells in an extended neighborhood that reflects typical downhill skiing behaviour.

The decision to move from one cell to another is determined by six environmental fields: slope, friction, boundary, curvature, aerodynamic drag, and inertia.

Slope and Friction The downhill gravitational component is captured via the slope field:

$$f_{\text{slope}} = 1 - \exp(-w_1 \sin \alpha), \tag{4}$$

where α is the slope angle and w_1 is a tunable weight.

Friction is modeled as

$$f_{\text{fric}}(i', j') = \exp\left(-w_2 \mu(i', j')\right), \tag{5}$$

where $\mu(i', j')$ is the local friction coefficient and w_2 regulates sensitivity.

Boundary Constraints Boundaries prevent skiers from leaving the piste. This is modeled using both a hard constraint and a soft constraint.

The hard constraint prevents movement beyond the slope width:

$$\tilde{P}(i', j')_\delta = 0, \quad \text{if } i' < 0 \text{ or } i' > M. \tag{6}$$

The soft constraint reduces transition probability near the edges:

$$f_{\text{boundary}}(i', j') = \exp\left(-w_3 \frac{1}{d_{\text{lat}}(i')}\right), \tag{7}$$

where

$$d_{\text{lat}}(i') = \min(i', M - i') \tag{8}$$

is the lateral distance from the candidate position to the slope boundary and w_3 is a sensitivity parameter.

Terrain Curvature The terrain curvature $\kappa_{i,j}$ at cell (i, j) is approximated using a discrete Laplacian:

$$\kappa_{i,j} = h_{i+1,j} + h_{i-1,j} + h_{i,j+1} + h_{i,j-1} - 4h_{i,j}, \tag{9}$$

where $h_{i,j}$ denotes the local elevation.

The curvature factor modifies transition probabilities:

$$f_{\text{curve}}(i', j') = \exp(w_4 \kappa_{i',j'}), \tag{10}$$

favoring concave regions and penalizing convex terrain structures.

Aerodynamic Drag Aerodynamic drag is modeled as a function of skier speed v_t:

$$f_{\text{air}}(i', j') = \exp(-w_5 v_t^2), \tag{11}$$

where w_5 is a tunable aerodynamic sensitivity parameter.

Directional Inertia To prevent unrealistic sharp turns, skier motion is constrained to directions

$$\delta \in \{-2, -1, 0, +1, +2\}$$

relative to the previous direction δ_{t-1}:

$$|\delta - \delta_{t-1}| \leq 1. \tag{12}$$

The inertia factor is defined as

$$I_\delta = \exp(-\gamma v_t |\delta - \delta_{t-1}|), \tag{13}$$

where γ modulates directional inertia strength.

Transition Probability The unnormalized transition probability for direction δ is

$$\begin{aligned}\tilde{P}_\delta = f_{\text{slope}}(i', j') \cdot f_{\text{fric}}(i', j') \cdot f_{\text{boundary}}(i', j') \\ \cdot f_{\text{curve}}(i', j') \cdot f_{\text{air}}(i', j') \cdot I_\delta.\end{aligned} \tag{14}$$

The normalized transition probability is

$$P_\delta = \frac{\tilde{P}_\delta}{\sum_{\delta' \in A} \tilde{P}_{\delta'}}, \tag{15}$$

where A is the set of admissible directions.

Speed Update The skier velocity is updated using an explicit Euler scheme:

$$v_{t+1} = v_t + \left(g \sin \alpha \cos \theta - \mu g \cos \alpha - c v_t^2\right) \Delta t, \tag{16}$$

where θ is the angle between the skier trajectory and the fall line, μ and c regulate resistance during turning and straight motion, and Δt denotes the simulation time step.

3.2. Behavioral and Skier-Specific Characteristics in Transition Modeling

To model heterogeneous skier behavior, we extend the baseline CA with skier-specific dynamics and multi-skier anticipation mechanisms.

3.2.1. Skier Ability and Motion Characteristics

A skier's skiing ability is measured by skiing skill, experience, piste difficulty, and turning technique [14]. Skiers with higher ability levels are generally more comfortable on steeper slopes, taking tighter turns, maintaining higher speeds, and navigating crowded or complex areas, reflecting greater confidence and proficiency on the slopes [13]. In the simulation, skiing ability influences transition probabilities by increasing the likelihood of selecting cells corresponding to sharper turns and reducing sensitivity to local congestion. We formalized the skiing ability by assigning each skier a discrete level $\ell_s \in \{\text{Beginner}, \text{Intermediate}, \text{Advanced}\}$.

Intrinsic Boldness We define a skier's intrinsic boldness, denoted B_s, as a personal characteristic that increases with skiing ability level. This represents the skier's willingness to take risks, overtake, or occupy more constrained paths.

Ability Level	Boldness B_s
Beginner	1.0
Intermediate	1.5
Advanced	2.0

3.2.2. Anticipation for Multi-Skier Interactions

To extend the cellular automaton model to multiple skiers, a behavioural anticipation factor is introduced to account for nearby skiers. Let skier s currently occupy cell (i, j) and let (i', j') denote a candidate next cell. Let O represent the set of nearby skiers within the local neighborhood. The anticipation factor $f_{\text{anticipation}}$ incorporates the intrinsic skier boldness B_s, such that bolder skiers are less deterred by nearby skiers.

Hard Constraint To prevent collisions, skiers must maintain a minimum separation distance $d_{\min}$ from one another. Candidate cells violating this constraint are rejected during the transition evaluation process:

$$d(i', j') < d_{\min}. \tag{17}$$

Soft Constraint When the hard constraint is satisfied, nearby skiers still influence the movement decision through a soft anticipation term. Let d_{safe} denote the anticipation range beyond which nearby skiers no longer influence the candidate transition. The anticipation factor is defined as

$$f_{\text{anticipation}}(i', j') = 1, \quad \text{if } d_{\min}(i', j') > d_{\text{safe}}, \tag{18}$$

and otherwise

$$f_{\text{anticipation}}(i', j') = \exp\left(-\frac{d_{\text{safe}}}{B_s\, d_{\min}(i', j')}\right). \tag{19}$$

The distance between the candidate cell (i', j') and skier o is computed using the distance metric

$$d(i', j', o) = \max\left(|i' - i_o|, |j' - j_o|\right), \tag{20}$$

and the minimum distance to nearby skiers is

$$d_{\min}(i', j') = \min_{o \in O} d(i', j', o). \tag{21}$$

The boldness parameter B_s modulates the strength of skier avoidance behaviour. Beginners (low B_s) experience stronger repulsion from nearby skiers and therefore perform larger avoidance manoeuvres, whereas advanced skiers (high B_s) tolerate smaller separation distances and maintain more direct downhill trajectories through local congestion. The anticipation factor is multiplicatively combined with the environmental and inertia-based transition factors described in Section 3.1.

3.3. Video-Consistent Trajectory Generation

We convert cellular automaton (CA) grid indices into metric world coordinates (X, Y, Z) representing a ski slope embedded in 3D space. The grid indices of the CA are defined so that j indexes motion along the slope and i indexes the across-slope direction (width). Downhill motion corresponds to decreasing j, while increasing i moves to the skier's right across the slope. Therefore, each cell represents a square patch on the slope surface. We place the CA origin at the top-left cell $(i_0, j_0) = (0, J - 1)$, where J denotes the number of cells along the slope direction.

Under this surface parameterization, across-slope and down-slope moves correspond to different 3D displacements even though the CA grid is uniform. In particular, across-slope motion is purely horizontal, while down-slope motion follows the inclined surface with an angle α. The CA lattice is embedded in a right-handed world coordinate frame (X, Y, Z), where X is the across-slope horizontal direction (positive to the right), Y is the horizontal downslope direction (ground-plane projection), and Z is vertical elevation (positive upward).

Let s denote the distance measured along the slope surface from the origin. For a planar incline, motion along the surface decomposes into horizontal and vertical components according to

$$\begin{aligned} Y &= s\cos\alpha, \\ Z &= -s\sin\alpha, \end{aligned} \tag{22}$$

where the negative sign reflects decreasing elevation in the downhill direction.

The along-slope distance associated with index j is

$$s_j = (j_0 - j)\, d, \tag{23}$$

while the across-slope displacement is

$$X_i = (i - i_0)\, d. \tag{24}$$

Combining these relationships yields the mapping from CA indices (i, j) to world coordinates:

$$\begin{aligned} X(i,j) &= (i - i_0)\, d, \\ Y(i,j) &= (j_0 - j)\, d \cos\alpha, \\ Z(i,j) &= -(j_0 - j)\, d \sin\alpha. \end{aligned} \tag{25}$$

Camera Projection The 3D world-space positions (X, Y, Z) are transformed into camera coordinates using the extrinsic parameters $(\mathbf{R}, \mathbf{t})$:

$$\begin{bmatrix} X^{\text{cam}} \\ Y^{\text{cam}} \\ Z^{\text{cam}} \end{bmatrix} = \mathbf{R} \begin{bmatrix} X \\ Y \\ Z \end{bmatrix} + \mathbf{t}. \tag{26}$$

The camera-space coordinates are projected to homogeneous image coordinates via the intrinsic matrix $\mathbf{K}$:

$$\begin{bmatrix} \tilde{u} \\ \tilde{v} \\ \tilde{w} \end{bmatrix} = \mathbf{K} \begin{bmatrix} X^{\text{cam}} \\ Y^{\text{cam}} \\ Z^{\text{cam}} \end{bmatrix}. \tag{27}$$

Finally, the 2D pixel coordinates (x, y) are obtained by:

$$x = \frac{\tilde{u}}{\tilde{w}}, \qquad y = \frac{\tilde{v}}{\tilde{w}}. \tag{28}$$

Depth-Consistent Bounding Boxes Assuming a skier height H and width W in meters, the projected dimensions are

$$h = \frac{f_y H}{\tilde{w}}, \qquad w = \frac{f_x W}{\tilde{w}}, \tag{29}$$

where f_x, f_y are the focal length. This guarantees correct perspective scaling, with skiers appearing larger when closer to the camera and smaller when farther away.

Temporal Resampling The CA timestep is set to $\Delta t_{\text{CA}} = 0.04\,\text{s}$ [17]. Since this timestep may differ from the target video frame rate, the projected trajectories are resampled using linear interpolation of the 2D coordinates, ensuring smooth motion without introducing discontinuities or artificial accelerations.

4. Experimental Evaluation

Our cellular automaton-based simulator produces visually plausible skier trajectories, as illustrated in Figure 1. We first analyze the influence of the anticipation mechanism and skier boldness parameters within the CA model. We then evaluate the quality of the generated data by assessing its usefulness for improving tracking performance and its similarity to real skier motion through comparison with the Slope-Track dataset [3].

4.1. Experimental Setup

4.1.1. Evaluation Protocol

Slope-Track Dataset The Slope-Track dataset [3] is a multi-object tracking benchmark for ski-slope environments, containing over 96,000 annotated frames collected across 10 ski resorts. The dataset includes bounding boxes and object identities and presents challenges such as small object sizes, frequent occlusions, and irregular skier motion patterns.

Tracking We employ DeepEIoU [7] together with the GlideTrack forecasting module and detection framework introduced in [3]. We retrained the GlideTrack module, while the detection model and the DeepEIoU tracking components remain unchanged from the configuration described in [3]. GlideTrack is a Mamba-based [4, 6] trajectory-forecasting module designed to improve skier tracking under occlusions or missed detections. GlideTrack is first pretrained on synthetic trajectory data generated by the CA simulation, providing a structured initialization prior to fine-tuning on Slope-Track. The synthetic pretraining data are generated using randomized slope geometries, skier densities, and camera configurations to increase motion diversity and improve generalization. Training uses AdamW with Smooth L1 and GIoU losses, together with random scaling and translation augmentations. The pretrained model is then fine-tuned on Slope-Track. Additional details on the synthetic data generation and training procedure can be found in the Supplementary Material Sec. 8.2.

4.1.2. Evaluation Metrics

CA Trajectory Efficiency Measures To investigate how anticipation and boldness influence skiing performance in the CA model, we evaluate the resulting motion dynamics using average speed, estimated sliding time, and total travelled distance. The physical and environmental conditions of the cellular automaton model were held constant except d_{safe}. Each configuration was run 50 times. Additional details on the experimental setup can be found in the Supplementary Material Sec. 8.1.

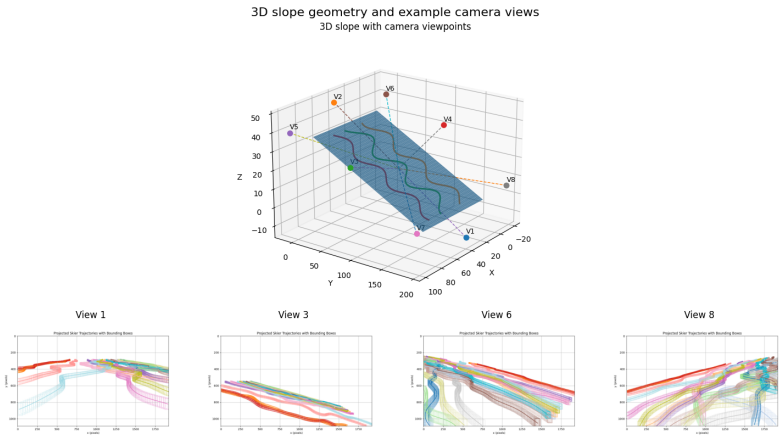

Figure 1. Camera configuration around the simulated ski slope. Top: 3D representation of the slope surface with example skier trajectories and the locations of virtual cameras (V1–V8). The camera positions are shown schematically for visualization purposes. In the simulation, most cameras are located near the slope edges (with varying heights in the Z direction), whereas the figure depicts them slightly offset from the slope for clarity. Dashed lines indicate the viewing direction of each camera. Bottom: Example 2D trajectory projections for selected camera views (View 1, View 3, View 6, and View 8).

Trajectory Distribution To compare the geometric characteristics of the generated and ground-truth trajectories, we analyze low-level normalized motion statistics. The normalized trajectory representation is examined using trajectory profiles and histograms for each variable. This captures the overall motion progression and spatial variability of the trajectories. Additional details can be found in the Supplementary Material Sec. 8.2.

Tracking The main metrics used to assess the usefulness of the synthetic data are standard multiple-object tracking metrics. The Higher Order Tracking Accuracy (HOTA) [11] jointly measures detection and association performance by computing the geometric mean of Detection Accuracy (DetA) and Association Accuracy (AssA) over matched tracks. AssA measures the correctness of temporal identity associations given correct detections, whereas DetA evaluates spatial detection accuracy independent of identity assignment. The Multi-Object Tracking Accuracy (MOTA) [2] measures overall tracking performance by penalizing three types of errors: missed detections, false detections, and identity switches. The IDF1 score evaluates identity preservation.

4.2. Experimental Results

4.2.1. Impact of Anticipation and Boldness

Figure 2 demonstrates the effect of anticipation on skier movement efficiency through average speed, sliding time, and total sliding distance. Figure 2b shows that increasing d_{safe} generally leads to higher skier speeds across all ability groups. Beginner and Intermediate skiers exhibit the largest increases in average speed as d_{safe} increases, whereas Advanced skiers maintain comparatively stable speeds across all anticipation distances because of their greater boldness and reduced sensitivity to nearby skiers.

Figure 2a demonstrates that larger anticipation distances generally reduce the total distance travelled by skiers. Lower d_{safe} values produce later local avoidance responses and increase the overall path length through larger lateral corrections and reactive manoeuvres. Figure 2c further supports the influence of anticipation on skier movement dynamics through variations in sliding time. Moderate increases in d_{safe} generally reduce the overall completion time, although the effect differs across ability groups. Beginner skiers show larger fluctuations in finish time because of their stronger sensitivity to nearby skiers, whereas Advanced skiers exhibit smaller changes in completion time because of their greater boldness and reduced sensitivity to local congestion.

4.2.2. Trajectory Distribution Analysis

Normalization The original slope geometry, camera calibration, and physical scale were not available in the annotated dataset, so a normalization procedure was applied to both real and simulated trajectories to enable meaningful comparison. Each trajectory is first expressed relative to its initial position, then rotated so that its dominant direction of motion aligns with the horizontal axis. The resulting along-track and lateral components are scaled to obtain normalized coordinates $(\tilde{c}_x, \tilde{c}_y)$. Bounding box dimensions are normalized in a similar way, yielding $(\tilde{w}, \tilde{h})$ that capture relative scale changes over time. This representation places all trajectories in a common coordinate system,

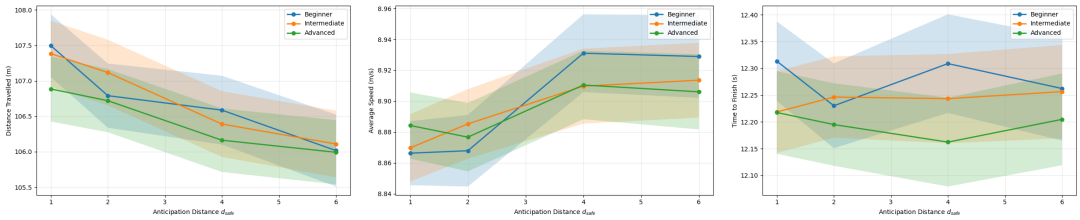

(a) (b) (c)

Figure 2. Effect of anticipation on skier movement efficiency for Beginner (1.0), Intermediate (1.5), and Advanced (2.0) skiers across 50 simulations with 30 skiers. The results show the mean average speed, total travelled distance, and sliding time for each ability group, with shaded regions representing the 95% confidence intervals.

allowing distributional analysis across different scenes and viewpoints. Further details are provided in the Supplementary Material Sec. 7, with an example shown in Figure 3.

Trajectory Profile Comparison Figure 4 presents the trajectory profiles and their variability for the normalized coordinates. The profiles summarize the lateral displacement $\tilde{c}_y$ as a function of normalized trajectory progress $\tilde{c}_x$ for both ground-truth (GT) and generated (GEN) trajectories. The shaded regions illustrate the variability of lateral motion around the central trajectory and provide a qualitative overview of the global trajectory structure.

The generated trajectories follow the same overall trend as the ground-truth data and reproduce the dominant lateral trajectory evolution reasonably well. However, the GT trajectories exhibit slightly larger lateral deviations and broader variability throughout portions of the trajectory progression. This indicates that the real trajectories contain a wider range of lateral motion behaviours and directional adjustments compared to the generated samples.

Distributional Statistics To further analyze the normalized trajectory representation, Figure 5 presents histograms of $\tilde{c}_x$, $\tilde{c}_y$, $\tilde{w}$, and $\tilde{h}$ for both datasets. These distributions provide a low-level comparison of the normalized trajectory variables and bounding-box dynamics between ground-truth and generated samples.

The distributions of $\tilde{c}_x$ for GT and GEN trajectories exhibit similar overall shapes, indicating that the simulator captures the general progression of motion along the dominant trajectory direction. However, the GT trajectories show a wider spread and heavier tails, whereas the GEN samples appear more concentrated, suggesting reduced variability in the simulated trajectory progression.

The distributions of $\tilde{c}_y$ for GT and generated trajectories are broadly similar, although the generated trajectories remain slightly more concentrated near zero, indicating smoother lateral motion on average. For the normalized bounding box dimensions $\tilde{w}$ and $\tilde{h}$, both datasets exhibit comparable central tendencies. However, the generated samples display slightly heavier tails, suggesting that the simulator produces a somewhat wider range of normalized bounding box variations than those observed in the ground-truth data.

Method	HOTA	IDF1	AssA	MOTA	DetA
train on *Slope-Track*					
DeepEIoU	65.0	66.7	58.4	74.2	72.4
DeepEIoU + G-T	68.1	70.9	63.8	74.6	72.7
pretrain on *Synthetic* & finetune on *Slope-Track*					
DeepEIoU + G-T	69.1	73.0	65.8	74.6	72.6

Table 1. Tracking performance of DeepEIoU with GlideTrack (G-T). The model is either trained solely on Slope-Track or initialized via synthetic pretraining and subsequently fine-tuned on Slope-Track.

4.2.3. Tracking Performance with Synthetic Data

Table 1 evaluates the impact of incorporating synthetic data on tracking performance using DeepEIoU with GlideTrack (G-T). Training solely on the Slope-Track dataset already provides a strong baseline. However, initializing the model with synthetic pretraining and subsequently fine-tuning on Slope-Track further improves several tracking metrics. In particular, performance increases to 69.1 HOTA, 73.0 IDF1, and 65.8 AssA, outperforming the model trained only on Slope-Track. These improvements suggest that synthetic pretraining introduces additional trajectory and motion variability, which improves identity consistency and object association across frames.

Additionally, detection-related metrics (MOTA and DetA) remain largely unchanged compared to the baseline. This indicates that the primary improvements arise from stronger temporal association and identity preservation rather than improved object detection quality.

5. Conclusion

This work presented a framework for generating synthetic skier trajectories for video-based applications. Building on a cellular automaton model, we incorporate skier-specific behaviors and anticipation mechanisms to model multi-

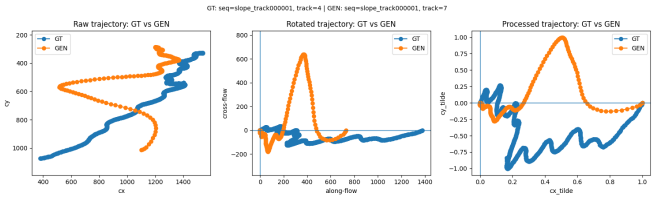

Figure 3. Example of trajectory processing for ground-truth (GT) and generated (GEN) tracks from one camera view. The example shows the raw trajectory in image coordinates, the trajectory rotated to align with the dominant motion direction, and the final normalized representation $(\tilde{c}_x, \tilde{c}_y)$ used for statistical comparison between real and generated trajectories.

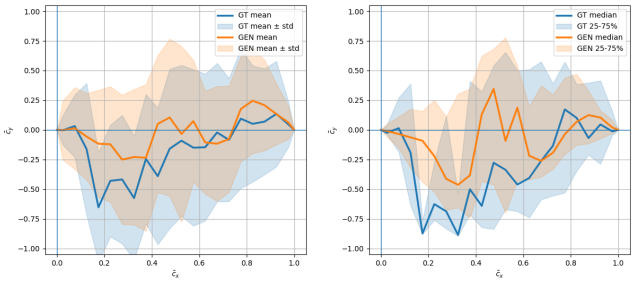

Figure 4. Mean and median trajectory profiles of normalized lateral displacement $\tilde{c}_y$ as a function of normalized trajectory progress $\tilde{c}_x$ for ground-truth (GT) and generated (GEN) trajectories. The shaded regions indicate variability around the central trajectory. **Left:** mean trajectory with one standard deviation. **Right:** median trajectory with interquartile spread (25–75%).

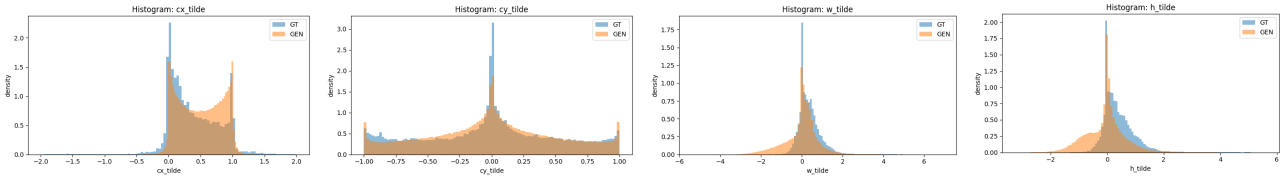

(a) $\tilde{c}_x$ (b) $\tilde{c}_y$ (c) $\tilde{w}$ (d) $\tilde{h}$

Figure 5. Histograms of normalized trajectory coordinates and bounding box dimensions for ground-truth (GT) and generated (GEN) trajectories.

skier interactions. The simulated trajectories are embedded in a 3D slope representation and projected into 2D image space using a virtual camera, enabling video-consistent synthetic observations.

Experiments show that synthetic trajectories provide useful training signals for tracking. Pretraining on synthetic data followed by fine-tuning on Slope-Track improves performance over training only on real data, particularly for association metrics. Detection metrics remain stable, indicating that the gains mainly arise from improved modeling of motion and trajectory dynamics.

The approach has several limitations. The simulation relies on simplified assumptions about slope geometry, skier dynamics, and skier behavior. Therefore, it cannot fully capture the variability of real skiing behavior. Rare events such as abrupt stops, falls, or collisions are not explicitly modeled. Skier skill level is used to determine a skier's boldness on the slope, but it fails to account for situations where an advanced skier is cautious or a beginner is reckless. In addition, a full comparison between real video trajectories and the generated trajectories could not be done as the exact calibration and scene geometry of the real dataset are unavailable.

Future work will focus on improving motion and projection accuracy through better slope and camera modeling, richer interaction behaviors, explicit modeling of rare events, and learning-based alignment between synthetic and real trajectory distributions.

6. Acknowledgements

This research is part of the collaborative i-Démo Régionalisé SOFTEN project (Solution pour l'Optimisation des Flux de skieurs pour la Transition ENergétique des domaines skiables) of the French government's regionalized France 2030 program. It was funded by BPI France, Direction Générale de la Compétitivité de l'Industrie et des Services (DGCIS), Grenoble Alpes Métropole and the Auvergne-Rhône-Alpes Region.

References

[1] Grzegorz Bazior, Jarosław Wkas, and Dariusz Pałka. Pedestrian dynamics model for high densities based on cellular automata. *Expert Systems with Applications*, 2025. 2

[2] Keni Bernardin and Rainer Stiefelhagen. Evaluating Multiple Object Tracking Performance: The CLEAR MOT Metrics. *EURASIP J. on Image and Video Process.*, pages 1–31, 2008. 6

[3] M'Saydez Campbell, Christophe Ducottet, Damien Muselet, and Rémi Emonet. Slope-track: Multiple object tracking on ski slopes. *Computer Vision and Image Understanding*, 264: 104663, 2026. 1, 5

[4] Tri Dao and Albert Gu. Transformers are SSMs: Generalized models and efficient algorithms through structured state space duality. In *International Conference on Machine Learning (ICML)*, 2024. 5

[5] A. García. On the modeling of dynamic queue formation and decision making in pedestrian systems. *Simulation Modelling Practice and Theory*, 2025. 2

[6] Albert Gu and Tri Dao. Mamba: Linear-time sequence modeling with selective state spaces. *arXiv preprint arXiv:2312.00752*, 2023. 5

[7] Hsiang-Wei Huang, Cheng-Yen Yang, Jiacheng Sun, Pyong-Kun Kim, Kwang-Ju Kim, Kyoungoh Lee, Chung-I Huang, and Jenq-Neng Hwang. Iterative Scale-Up ExpansionIoU and Deep Features Association for Multi-Object Tracking in Sports. In *Proc. of the IEEE/CVF Winter Conf. on Appl. of Comput. Vis.*, pages 163–172, 2024. 1, 5

[8] Nan Jiang, Eric Wai Ming Lee, L. Yang, Richard K. K. Yuen, and C. Zhai. A deep-learning-based approach for simulating pedestrian turning flow. *Expert Systems with Applications*, 262:125706, 2025. 1

[9] Jong Wook Kim and Beakcheol Jang. Deep learning-based privacy-preserving framework for synthetic trajectory generation. *Journal of Network and Computer Applications*, 206: 103459, 2022. 1

[10] Tong Lu, Yuxin Zhang, Weikang Xie, and Xinyan Huang. Human-ai interactive framework for smart evacuation safety analysis in large infrastructures. *Reliability Engineering I& System Safety*, 266:111695, 2026. 1

[11] Jonathon Luiten, Aljosa Osep, Patrick Dendorfer, Philip Torr, Andreas Geiger, Laura Leal-Taixé, and Bastian Leibe. HOTA: A Higher Order Metric for Evaluating Multi-Object Tracking. *Int. J. of Comput. Vis.*, pages 1–31, 2020. 6

[12] Wei Lv, Jinghui Wang, Zhiming Fang, and Dun Mao. Simulation method of urban evacuation based on mesoscopic cellular automata. *arXiv preprint arXiv:2311.10554*, 2023. 2

[13] Günter Ruedl, E Pocecco, R Sommersacher, H Gatterer, M Kopp, W Nachbauer, and M Burtscher. Factors associated with self-reported risk-taking behaviour on ski slopes. *British Journal of Sports Medicine*, 44(3):204–206, 2010. 4

[14] Steinar Sulheim, Arne Ekeland, and Roald Bahr. Self-estimation of ability among skiers and snowboarders in alpine skiing resorts. *Knee Surgery, Sports Traumatology, Arthroscopy*, 15(5):665–670, 2007. 4

[15] Anita et al. Ullrich. A hybrid workflow connecting a network and an agent-based model for predictive pedestrian movement modelling. *Frontiers in Built Environment*, 2024. 2

[16] Jinghui Wang and Wei Lv. Cosforce: A force-based general model considering pedestrian anticipation and reaction mechanisms. *arXiv preprint arXiv:2410.10746*, 2024. 1

[17] Buchuan Zhang and Chuan-Zhi Thomas Xie. Exploring the complexity of pedestrian dynamics in skiing: A modelling and simulation framework. *Simulation Modelling Practice and Theory*, 146:103225, 2026. 2, 3, 5

[18] Buchuan Zhang, Tim Dressler, Alexander Maurer, Michael Nader, and Andreas Schadschneider. Simulation of downhill skiing areas. *Collective Dynamics*, 9:1–7, 2024. 1

[19] et al. Zhang. Development of the social force model considering pedestrian characteristics. *Transportation Research Record*, 2023. 1